doi:10.1093/brain/awp023 Brain 2009: 132; 1335–1345 | 1335

BRAIN
A JOURNAL OF NEUROLOGY

Amyloid-dependent triosephosphate isomerase nitrotyrosination induces glycation and tau fibrillation

Francesc X. Guix,[1,2] Gerard Ill-Raga,[1] Ramona Bravo,[3] Tadashi Nakaya,[4] Gianni de Fabritiis,[5] Mireia Coma,[1] Gian Pietro Miscione,[5] Jordi Villà-Freixa,[5] Toshiharu Suzuki,[4] Xavier Fernàndez-Busquets,[3] Miguel A. Valverde,[1] Bart de Strooper[2,6] and Francisco J. Muñoz[1]

1 Laboratory of Molecular Physiology and Channelopathies, Department of Experimental and Health Sciences, Universitat Pompeu Fabra (UPF), Barcelona, Spain
2 Department for Developmental and Molecular Genetics–VIB, Leuven, Belgium
3 Biomolecular Interactions Team, Institute for Bioengineering of Catalonia, and Nanoscience and Nanotechnology Institute, University of Barcelona, Spain
4 Laboratory of Neuroscience, Graduate School of Pharmaceutical Sciences, Hokkaido University, Sapporo, Japan
5 Unitat de Recerca en Informàtica Biomèdica, UPF-Institut Municipal d'Investigació Mèdica, Barcelona, Spain
6 Center for Human Genetics, Leuven, Belgium

Correspondence to: Dr Francisco J. Muñoz,
Grup de Fisiologia Molecular i Canalopaties,
Departament de Ciències Experimentals i de la Salut,
Universitat Pompeu Fabra,
C/ Dr Aiguader, 88,
08003 Barcelona, Spain
E-mail: paco.munoz@upf.edu

Alzheimer's disease neuropathology is characterized by neuronal death, amyloid β-peptide deposits and neurofibrillary tangles composed of paired helical filaments of tau protein. Although crucial for our understanding of the pathogenesis of Alzheimer's disease, the molecular mechanisms linking amyloid β-peptide and paired helical filaments remain unknown. Here, we show that amyloid β-peptide-induced nitro-oxidative damage promotes the nitrotyrosination of the glycolytic enzyme triosephosphate isomerase in human neuroblastoma cells. Consequently, nitro-triosephosphate isomerase was found to be present in brain slides from double transgenic mice overexpressing human amyloid precursor protein and presenilin 1, and in Alzheimer's disease patients. Higher levels of nitro-triosephosphate isomerase ($P<0.05$) were detected, by Western blot, in immunoprecipitates from hippocampus (9 individuals) and frontal cortex (13 individuals) of Alzheimer's disease patients, compared with healthy subjects (4 and 9 individuals, respectively). Triosephosphate isomerase nitrotyrosination decreases the glycolytic flow. Moreover, during its isomerase activity, it triggers the production of the highly neurotoxic methylglyoxal ($n=4$; $P<0.05$). The bioinformatics simulation of the nitration of tyrosines 164 and 208, close to the catalytic centre, fits with a reduced isomerase activity. Human embryonic kidney (HEK) cells overexpressing double mutant triosephosphate isomerase (Tyr164 and 208 by Phe164 and 208) showed high methylglyoxal production. This finding correlates with the widespread glycation immunostaining in Alzheimer's disease cortex and hippocampus from double transgenic mice overexpressing amyloid precursor protein and presenilin 1. Furthermore, nitro-triosephosphate isomerase formed large β-sheet aggregates *in vitro* and *in vivo*, as demonstrated by turbidometric analysis and electron microscopy. Transmission electron microscopy (TEM) and atomic force

Received August 6, 2008. Revised January 11, 2009. Accepted January 15, 2009. Advance Access publication February 27, 2009

microscopy studies have demonstrated that nitro-triosephosphate isomerase binds tau monomers and induces tau aggregation to form paired helical filaments, the characteristic intracellular hallmark of Alzheimer's disease brains. Our results link oxidative stress, the main etiopathogenic mechanism in sporadic Alzheimer's disease, via the production of peroxynitrite and nitrotyrosination of triosephosphate isomerase, to amyloid β-peptide-induced toxicity and tau pathology.

Keywords: Alzheimer's disease; amyloid β-peptide; tau protein; triosephosphate isomerase; peroxynitrite

Abbreviations: AFM = Atomic Force Microscopy; DHAP = dihydroxyacetone phosphate; GAP = D-glyceraldehyde 3-phosphate; NFT = neurofibrillary tangles; PHF = paired helical filaments; PS1 = presenilin 1; SIN-1 = peroxynitrite donor; TEM = Transmission electron microscopy; TPI = triosephosphate isomerase

Introduction

Since the characterization of amyloid β-peptide (Aβ) deposition (Masters and Beyreuther, 2006) and the subsequent formation of neurofibrillary tangles (Iqbal *et al*., 1984; Brion *et al*., 1985) as the two defining pathological hallmarks of Alzheimer's disease, a fair amount of research on Alzheimer's disease has been directed towards the identification of the molecular mechanism linking Aβ and neurofibrillary tangles. Interestingly, aggregation of Aβ (either in oligomeric or insoluble mature fibrils) is mainly extracellular while neurofibrillary tangles (composed of paired helical filaments of tau protein) appear intracellularly (Gotz *et al*., 2001; Alonso *et al*., 2008). In addition to this spatial segregation, Aβ accumulation and neurofibrillary tangles also show temporal separation in Alzheimer's disease brains, i.e. Aβ accumulation appears before neurofibrillary tangles (Gotz *et al*., 2001; Del Toro *et al*., 2005). Altogether, the existing data suggest a hierarchical relationship between Aβ and tau, although the underlying mechanisms are unknown. The activation of phosphorylation pathways (Otth *et al*., 2002; Liou *et al*., 2003; Bhat *et al*., 2004) is the current hypothesis associating Aβ and paired helical filaments, but the fact that paired helical filament formation can occur in the absence of tau phosphorylation (Mudher and Lovestone, 2002; Chang *et al*., 2008) suggests that phosphorylation is an enhancer of tau fibrillization rather than a trigger (Kuret *et al*., 2005). Thus, the crucial questions of what unleashes paired helical filament formation and which are the mechanisms linking Aβ and paired helical filaments remain unanswered at the molecular level.

Alzheimer's disease, as other amyloidoses, presents insoluble accumulations of β-sheet containing proteins, which otherwise should be soluble in biological fluids. A widely accepted view is that the process is entirely pathological, requiring triggers that relieve the conformational barrier to spontaneous protein aggregation. These can be of genetic origin, e.g. disease-causing mutations in the proteins themselves or in regulators of their metabolism. In the case of the tau protein, mutations in its encoding gene do not generate Alzheimer's disease, but are responsible for another neurodegenerative disorder known as frontotemporal dementia with Parkinsonism (reviewed in Wszolek *et al*., 2006). Alternatively, increased expression of tau protein, together with changes in the cellular environment such as the presence of agents that act as seeds for heterogeneous nucleation and aggregation (anionic surfactants and polyanions) (Chirita *et al*., 2003; Sibille *et al*., 2006), can induce tangle formation. However, none of these mechanisms have provided insight into the molecular link between Aβ and neurofibrillary tangles.

Triosephosphate isomerase (TPI) is a key enzyme in cell metabolism that controls the glycolytic flow and energy production through the interconversion of dihydroxyacetone phosphate (DHAP) and D-glyceraldehyde 3-phosphate (G3P) (Richard, 1993). Notably, TPI is the only glycolytic enzyme whose functional deficiency is associated to neurodegeneration (Eber *et al*., 1991; Ovadi *et al*., 2004). In particular, inefficient glycolysis (Hoyer *et al*., 1988) and ATP depletion (Keil *et al*., 2004) are characteristic in Alzheimer's disease brains. Nitrotyrosination of TPI occurs in Alzheimer's disease (Coma *et al*., 2005) as the result of Aβ-dependent oxidative stress due to the formation of the powerful nitrating agent peroxynitrite by the reaction of nitric oxide and superoxide anion (Coma *et al*., 2005; Guix *et al*., 2005).

Here, we have discovered a mechanism that can account for the spatial and temporal progression from Aβ toxicity to neurofibrillary tangles in Alzheimer's disease brain. Aβ-induced oxidative and nitrative stress induces nitrotyrosination of TPI, a key enzyme of the glycolytic pathway. This causes the generation of toxic intermediates and abnormal glycation of proteins, as well as a conformational change in TPI itself, making it prone to aggregate. More interestingly, the nitrotyronisated TPI is able to induce a conformational change in tau and precipitates paired helical filament formation.

Materials and Methods

Materials

Synthetic Aβ peptide corresponding to the human $A\beta_{1-42}$ sequence was purchased from AnaSpec. Rabbit TPI, SIN-1 and Protein G immobilized on sepharose were purchased from Sigma-Aldrich.

Human brain samples

Human brain tissue sections and samples were supplied by the Banc de Teixits Neurològics (Serveis Científico-Tècnics, Hospital Clínic, Universitat de Barcelona), the Unitat d'Anatomia Patològica (Hospital del Mar) and the Unitat de Nauropatología y Banco de Cerebros (Fundación Hospital Alcorcón). The procedure was approved by the Ethics Committee of the Institut Municipal d'Investigacions Mèdiques-Universitat Pompeu Fabra. Brain sections (5 μm) were obtained from the frontal cortex of four healthy aged individuals and five Alzheimer's disease patients at stage VI. Brain samples from the frontal cortex of two individuals with

Parkinson's disease and two with frontotemporal dementia were also used in the study. Samples used in the biochemical studies were from nine control individuals and 13 Alzheimer's disease patients. Five hundred milligram of either frontal cortex or hippocampus was homogenized at 4°C with 500 µl of a cocktail containing 480 µl NP40 lysis buffer (150 mM NaCl, 5 mM EDTA, 1% Nonidet P-40, 1 mM sodium orthovanadate, 1 mM phenylmethylsulphonyl fluoride, 0.05% aprotinin, 1 mM dithioltreitol) and 120 µl of protease inhibitors (Complete mini-EDTA free) from Roche Diagnostics GmbH. Lysates were shaken at 4°C for 30 min and centrifuged at 13 000 r.p.m. for 15 min. Proteins in the supernatant were quantified with the Bradford assay.

Mice brain samples

Cerebral paraffined slides from wild-type black mice or APPswe/PS1 L166P mice were deparaffined with Clear Rite 3 and subsequent washes with decreasing ethanol dilutions. The Tyramide Signal Amplification kit (Perkin-Elmer) was used for the immunofluorescence, following the instructions given by the company. Briefly, slides were incubated for 7 min with a 70% formic acid solution to expose the epitopes. After 1 h of quenching endogenous peroxidase activity with a 30% H_2O_2 solution, slides were blocked for 1 h at room temperature with 2% normal serum in TNB blocking buffer. The same solution was used to dilute (1 : 100) the following primary antibodies: anti-TPI (ProteinTech Group, Chicago), 6E10 anti-Aβ, anti-MG (CosmoBio) and anti-nitrotyrosine (Abcam). The primary antibodies were incubated overnight at 4°C. The secondary antibodies were diluted (1 : 500) in TNB blocking solution without serum with the exception of the anti-MG, which was diluted 1 : 200. Slides were developed by 6-min incubation with the Tyr-FITC reagent at darkness (1 : 50 in 1× reagent diluent). All the washes were performed with TNT 1× buffer. For the TPI-amyloid co-localization study a HRP-bound antibody against rabbit was used. For the MG-amyloid co-localization study a HRP-bound antibody against mouse was used together with a co-staining with thioflavine T to detect amyloid deposits.

Western blot

Gels were transferred to nitrocellulose membranes and incubated for 2 h at room temperature with a rabbit anti-nitrotyrosine polyclonal antibody (1 : 1000, Invitrogen), a sheep anti-TPI polyclonal antibody (1 : 200, Nordic), a mouse anti-tau monoclonal antibody (1 : 1000, Santa Cruz) or a mouse anti-argpyrimidine antibody (1 : 1000, CosmoBio). Donkey anti-rabbit and donkey anti-sheep peroxidase-conjugated secondary antibodies (1 : 5000, Amersham Bioscience) were incubated for 1 h at room temperature. Bands were visualized using the enhanced chemiluminescence substrate (Super Signal; Pierce) and the Hyperfilm ECL kit from Amersham Bioscience.

Immunoprecipitation

Total protein (500 µg) from brains or SH-SY5Y cells (human neuroblastoma cells) lysates were incubated with 1.25 µg of anti-TPI polyclonal antibody overnight at 4°C. Following the addition of protein G immobilized on sepharose (Sigma), samples were shaken for 2 h at room temperature. Aggregates were pulled down by centrifugation at 10 000 r.p.m. for 10 min and washed thrice. Protein G and antibody were removed from the immunoprecipitated proteins by boiling the samples for 6 min at 100°C.

Quantification of nitrotyrosinated TPI in brains

TPI was inmunoprecipitated from either cerebral cortex or hippocampus of control and Alzheimer's disease patients. Samples were resuspended in 100 µl of basic PBS (pH 12) and boiled before the removal of protein G by centrifugation. The absorbance was then measured at 420 nm to determine the amount of nitrotyrosines in the samples. Free nitrotyrosine (Sigma) was used to make a standard curve.

Immunohistochemistry and immunofluorescence

Frontal cortex sections were pretreated with 50% formic acid for 1 min to expose TPI epitopes. Sections were treated with 4% H_2O_2 and incubated with rabbit anti-nitrotyrosine polyclonal antibody (1 : 500) for 2 h at room temperature followed by incubation with donkey anti-rabbit peroxidase-conjugated antibody (1 : 500) for 1 h at room temperature. Contiguous sections were incubated with sheep anti-TPI polyclonal antibody (1 : 100) and donkey anti-sheep peroxidase-conjugated antibody (1 : 500) for 1 h at room temperature. Slides were treated with Peroxidase Substrate Kit DAB (Vector). Samples were counterstained with haematoxylin, dehydrated and fixed with Eukitt (O. Kindler GmbH &CO). Representative digital images were taken with a Leica DMR microscope and analysed with Leica IM50 software. To demonstrate the presence of methylglyoxal in the human samples from Alzheimer's disease brains the slides were analysed by immunofluorescence following the protocol previously mentioned. The content of methylglyoxal was determined with an anti-MG monoclonal antibody. The immunofluorescence experiment on tissue slides was performed as explained previously for the mice brain samples.

For the immunofluorescence experiment on TPI aggregates two different secondary antibodies were used: an Alexa568-bound rabbit antibody for TPI and an Alexa488-bound mouse antibody for tau. As a negative control a primary antibody against human syntaxin 1A was used.

Overexpression of TPI in HEK cells

TPI was amplified by PCR from purified human chromosomal DNA and cloned into a construct containing a 5′ upstream Flag sequence. A TPI carrying double tyrosine mutation (Y164F/Y208F) was generated and cloned into the same construct. HEK cells were seeded in six-well plates at a density of 500 000 cells per well and grown for 12 h with Dulbecco's modified Eagle's medium (DMEM) supplemented with 10% FBS. Afterwards, 2 µg per well of each construct was transfected using 2 µl Lipofectamine 2000 (Invitrogen). After 24 h, the medium was substituted by DMEM without FBS and cells were treated with 0.5 µM pre-aggregated Aβ or left without treatment (mock). After 24 h, cells were lysed and TPI was inmunoprecipitated with an anti-Flag antibody (Sigma). A Western blot was run and an anti-nitrotyrosine antibody used to visualize the bands.

TPI nitration *in vitro*

Rabbit TPI (1.25 µg/µl unless otherwise indicated) was dissolved in 50 mM tetraethylammoniun (pH 7.4–7.6) and exposed to SIN-1 at the concentrations specified in each assay. The nitration process was

carried out by shaking at 300 r.p.m. for 3 h at room temperature. SIN-1 was eliminated from the samples with a PD-10 desalting column (Amersham). The elution profile is shown in the supplementary material.

Kinetic studies and methylglyoxal measurement

The isomerase activity of TPI was measured spectrophotometrically using glyceraldehyde 3-phosphate (G3P) or dihydroxyacetone phosphate (DHAP) as substrates and coupling the products obtained to α-glycerophosphate dehydrogenase or G3P dehydrogenase, respectively. The final volume was 500 µl in both cases. The assay mixture for the G3P to DHAP direction contained 50 mM triethanolamine/HCl (pH 7.6), 0.2 mM NADH, 0.1 mM EDTA, D,L-G3P (1, 0.5, 0.33, 0.2 and 0.05 mM), 3 ng of TPI and 0.9 U of α-glycerophosphate dehydrogenase. The assay mixture for the DHAP to G3P direction contained 50 mM triethanolamine/HCl (pH 7.4), 0.72 mM NAD^+, 0.47 mM Na_3AsO_4, DHAP (0.3, 0.6, 1.2, 2.4, 4.8 and 9.5 mM), 10 ng of TPI and 3.24 U of α-glycerophosphate dehydrogenase. Methylglyoxal generated during the isomerization reaction was quantified enzymatically, in both reactions, through conversion to *S*-lactoyl glutathione by glyoxalase I, and the reaction was followed spectrophotometrically at 240 nm. Initial velocity mean for each substrate concentration was transformed to be plotted on an Eadie-Hofstee graph (to calculate K_m) or on a Woolf-Hanes graph (to calculate V_{max}). Values of $P<0.05$ were obtained for all the parameters of the linear regression models after student's *t*-test statistical analysis.

Computational modelling of TPI

The crystal structure was downloaded from the PDB data bank (PDB:8TIM). Using the package VMD, chain A was selected for the molecular dynamics simulations. The protein was solvated in TIP3P water and ion to neutralize the charge for a total system size of around 50 000 atoms. Using the molecular dynamics package NAMD2.6 (NAMD), the protein restrained with a harmonic potential of 25 kcal/mol, the entire system was energy minimized for 1000 steps and thermalized, reinitializing atom velocities twice. The constrained was then removed and the system equilibrated for a further 10 ps. Finally a Langevin piston barostat at 1 atm was applied for 3 ns. The production run consisted of 4 ns of simulation in the same condition. The most important simulation parameters setting were: time step of 2 fs, a cut of 12 A and update of the pairlist every 20 iterations, long-range forces are computed every 4 fs and long-range electrostatic was resolved with the PME method with at least one grid point each Angstrom. Four tyrosines were present for each monomer of TPI. The first two Y47 and Y67 stays at the interface of the dimer in opposite orientations, such that tyrosines from different monomers do not face each other, while the remaining two Y164 and Y208 are interacting directly and sit very close to the catalytic site E165 and a large loop overshadowing the catalytic site formed by at least K13, H95 and E165. Y208 is hydrogen bonded with A176 in this loop, effectively shortening the length of the loop with a short pinch. The deprotonated tyrosines were modelled by removing the hydrogen atom of the hydrophilic end of the tyrosines Y164 and Y208 and by assigning a total-1 charge to each. The other two tyrosines, far away from the catalytic site, are left in the native state. From the equilibrated structure a 10-ns simulation with the deprotonated tyrosines was run.

Turbidometric analyses

Turbidometric experiments were carried out at room temperature, within a dark chamber in a 96-well plate under continuous shaking (300 r.p.m.). The protein concentration of the wells containing rabbit TPI or bovine RNase was 2.5 µg/µl. Final volume for all the wells was 100 µl. Specific conditions for each well are indicated in the legend of Fig. 3.

Thioflavin staining

Control and nitrotyrosinated TPI were shaken at 300 rpm and at room temperature for 1 day or 5 days. Before microscope observation, Thioflavin T (1 mM) was added to each sample at 1 : 1 (v/v) and incubated in darkness for 15 min. Samples were placed on coverslips and examined under blue light with a Leica DMR microscope coupled to a DFC300 FX camera. Representative images were taken with the Leica IM50 software.

Transmission electron microscopy

Mesh nickel grids were charged with UV light for 5 min and set on a drop of sample for 1 min. Three consecutive washes with milliQ water were carried out (1 min in total). Finally the grid was set on a drop of 2% uranil acetate solution for 1 min and dried. Samples were observed with a Jeol 1010 electron microscope.

Atomic force microscopy

Imaging was performed with a commercial MultiMode atomic force microscope controlled by a Nanoscope IV electronics (Digital Instruments) equipped with either a 12-µm scanner (E-scanner) or a 120-µm scanner (J-scanner). Except where otherwise indicated, all images were taken in liquid using a tapping-mode liquid cell without the O-ring seal. Oxide-sharpened pyramidal Si_3N_4 tips mounted on triangular 100-µm long cantilevers ($k = 0.08$ N/m) were purchased from Olympus. The liquid cell and the tip were cleaned with ethanol and thoroughly rinsed with deionized water before use. For high-resolution imaging the microscope head was placed on a vibration-isolated stone plate. After the indicated incubation times and immediately before imaging, 10 µl of the sample were allowed to adsorb for about 5–10 min at room temperature on freshly cleaved muscovita mica (Asheville-Schoonmaker Mica Co.) or highly ordered pyrolytic graphite (Nt-MDT Co.), and finally overlaid with ~100 µl of incubation buffer.

Confocal microscopy

TPI immunoprecipitated from healthy or Alzheimer cortex was immobilized on microscope coverslides coated with gelatin (5% in deionized water). Samples were fixed with a solution of 4% formaldehyde for 30 min and incubated for 2 h at room temperature with a mouse anti-phospho-tau monoclonal antibody (1 : 1000 Innogenetics) followed by incubation with Alexa fluor 488 goat anti-mouse polyclonal antibody (1 : 500) for 1 h at room temperature. Digital images were taken with a Leica TCS SP confocal microscope and analysed with Leica confocal software.

Results

Aβ promotes TPI nitrotyrosination *in vitro* and in Alzheimer's disease

Aβ induced nitro-oxidative stress on human neuroblastoma cells, resulting in nitrotyrosination of TPI (Fig. 1A). Double transgenic mice overexpressing amyloid precursor protein (APP) and presenilin 1 (PS1), showed TPI aggregates (Fig. 1B) and nitrotyrosination (Fig. 1C) in identical hippocampal areas. Similarly, co-localization of TPI (Fig. 1D) and anti-nitrotyrosine staining (Fig. 1E) was found in the parenchyma of human Alzheimer's disease brains. Moreover, higher levels of nitro-TPI were also detected in extracts from hippocampus (Fig. 1F) and frontal cortex (Fig. 1G) obtained from Alzheimer's disease brains, compared with healthy subjects.

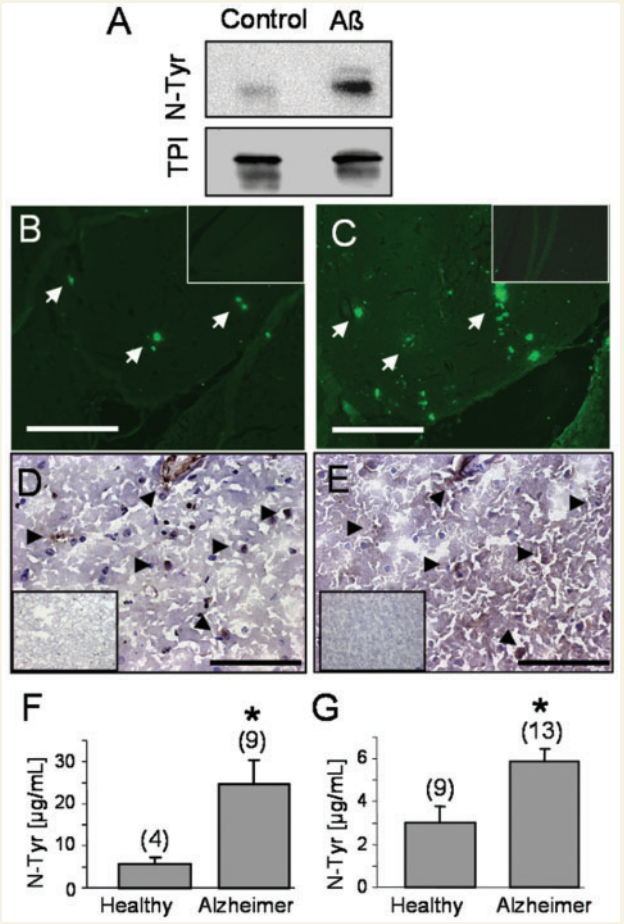

Figure 1 TPI nitrotyrosination is dependent on the presence of Aβ. (**A**) SH-SY5Y cells were treated with 1 μM $A\beta_{1-42}$ and TPI was immunoprecipitated. Blots were performed with either anti-nitrotyrosine or anti-TPI antibodies. (**B** and **C**) Hippocampus from double transgenic mice overexpressing APP and PS1, and (**D** and **E**) frontal cortex sections obtained from Alzheimer's disease brain patients were immunostained with antibodies against (**B** and **D**) TPI or (**C** and **E**) against nitrotyrosine. No staining is shown in wild-type mice for (inset **B**) TPI and (inset **C**) nitrotyrosine, and in healthy human controls for (inset **D**) TPI and (inset **E**) nitrotyrosine. Bars are 250 μm (**B** and **C**) and 98 μm (**D** and **E**). TPI was immunoprecipitated from healthy and Alzheimer's disease (**F**) hippocampus or (**G**) cortex and nitrotyrosine was measured. The number of independent samples is indicated between brackets; $^*P<0.05$ by student's *t* analysis.

Aβ-induced TPI nitrotyrosination causes a loss of enzymatic specificity

TPI has four Tyr residues. Tyr164 and Tyr208 are more prone to modification by nitric oxide because they are in the proximity of negative charged amino acids and also more exposed to the external agent (Supplementary Fig. S1). We modelled the functional consequences of TPI nitrotyrosination using full-atom molecular dynamics. The loop 6 (Supplementary Fig. S1) is very flexible and plays an important role in the reactivity of the enzyme (Alber *et al*., 1981). Nitration of Tyr164 and Tyr208 would destabilize the closed state of loop 6 because the interaction between Tyr208 and Ala176 through an H-bond would be compromised (Fig. 2A and B; Supplementary Fig. S2). Indeed, purified TPI after nitrotyrosination with a peroxynitrite donor (SIN-1) displayed a significant decrease in isomerase activity in both directions of the catalysis, i.e. using DHAP (Fig. 2C) or GAP (Fig. 2D) as substrate. A significant reduction in the catalytic parameters was also obtained for nitro-TPI (Table 1; Supplementary Fig. S3). Decreased isomerase activity should slow the glycolytic flow and reduce ATP formation. The isomerization of DHAP and GAP proceeds through an enediol phosphate. This intermediate is very unstable and can suffer ω-elimination of the phosphate group to yield inorganic phosphate and methylglyoxal (Richard, 1993; Ovadi *et al*., 2004). Methylglyoxal is a toxic compound involved in advanced glycation end-product formation (Richard, 1993; Kuhla *et al*., 2005). In accordance with the decreased efficiency of nitro-TPI we found a significant increase in methylglyoxal production ($P<0.05$), independent of whether DHAP or GAP was used as substrate (Fig. 2E). Thus, nitrotyrosination of TPI results in reduced catalytic activity and increased occupancy of the enzyme by the substrate, and consequently, a higher production of the toxic methylglyoxal. This hypothesis was confirmed using HEK cells overexpressing wild-type and mutant TPI (Tyr164Phe and Tyr208Phe mutations that mimic the effect of nitrotyrosination on loop stability). Mutant TPI showed increased methylglyoxal production, detected by Western blots using anti-argpyrimidin which recognizes products of aminoacid glycation (Fig. 2F).

Interestingly, brains of double transgenic mice showed overlapping Aβ deposits (Fig. 3A and C) with TPI (Fig. 3B) and methylglyoxal positive areas (Fig. 3D) in the hippocampus. Moreover TPI (Fig. 3E) co-localized with methylglyoxal (Fig. 3F) in mice. Methylglyoxal levels were significantly higher in human Alzheimer's disease brains (Fig. 3H) than in healthy controls (Fig. 3G), corroborating the pathological significance of our biochemical findings.

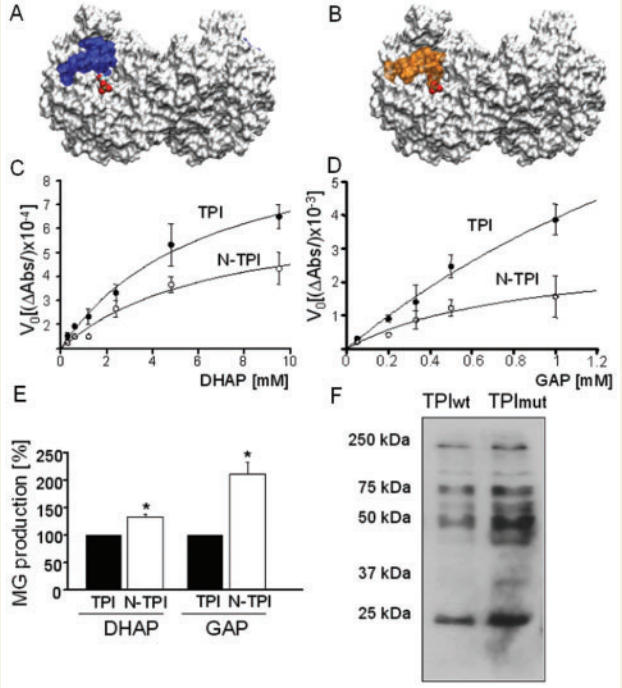

Figure 2 TPI nitrotyrosination induces a decrease in its isomerase activity but an increase in methylglyoxal production. (**A**) The solvent surface accessible area (SASA) of the TPI enzyme (PDB:1NEY) in its dimer conformation is computed over the average conformation of a multi nanosecond trajectory of a molecular dynamics run (white surface) bound with the DHAP substrate in the catalytic site. (**B**) The same loop is plotted in orange in a similar simulation but introducing nitrated tyrosines at 164 and 208. In average the loop assumes a more closed conformation. Nitrotyrosination decreases the catalytic efficiency of TPI. The activity of control and nitrotyrosinated TPI was measured in both directions (**C**) from DHAP to GAP and (**D**) from GAP to DHAP. The respective Michaelis-Menten curves show that the nitrotyrosination of TPI produces a significant decrease in the TPI isomerase activity of the enzyme. $n = 3$–5 experiments for each point. (**E**) Methylglyoxal production by TPI or nitro-TPI using DHAP or GAP as initial substrates. $n = 4$ independent experiments; $^{*}P < 0.05$ by student's t analysis. (**F**) Western blot analysis of methylglyoxal production using anti-argpyrimidin, which recognizes glication products. Protein extract (100 μg) from HEK cells overexpressing WT (first lane) or double mutant (Tyr164 and 208 by Phe164 and 208) TPI were applied.

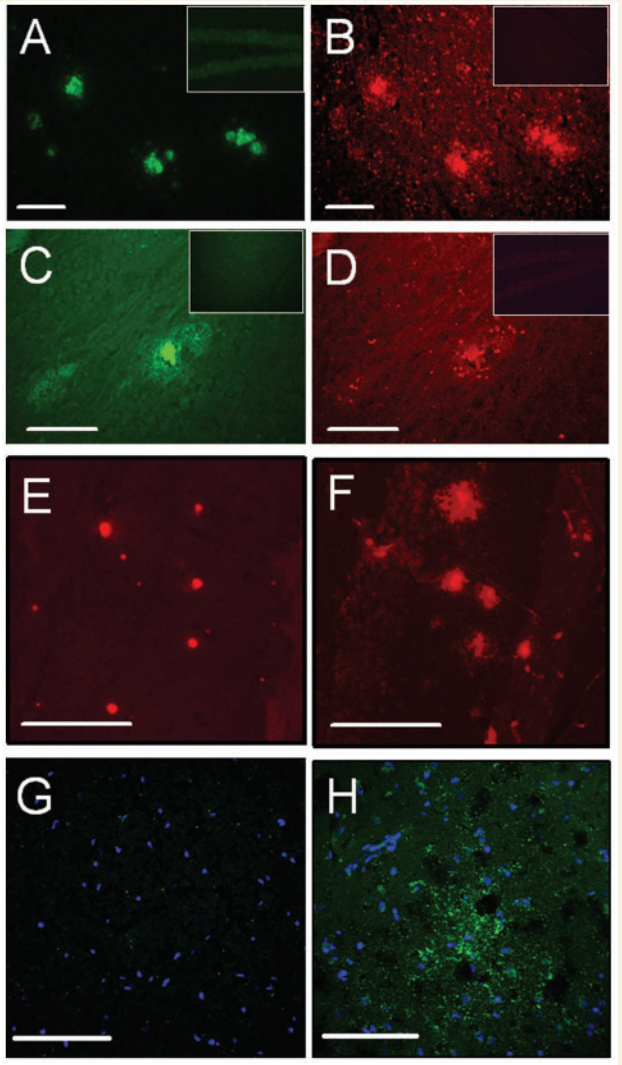

Figure 3 Methylglyoxal production is increased in APP-PS1 double transgenic mice and Alzheimer's disease patients. Consecutive serial hippocampal sections from double transgenic mice were immunostained to demonstrate the presence of (**A**) Aβ and (**B**) TPI; (**C**) Aβ identified by thioflavine T staining and (**D**) methylglyoxal; and, (**E**) TPI and (**F**) methylglyoxal. Controls with wild-type mice were performed for (insets **A** and **C**) Aβ, (inset **B**) TPI and (inset **D**) methylglyoxal. Cortex samples from (**G**) healthy and (**H**) Alzheimer's disease patients were immunostained with anti-MG antibody producing green fluorescence. Nuclei were stained in blue. Bars are 75 μm (**A**–**D**), 125 μm (**E** and **F**) and 250 μm (**G** and **H**).

Table 1 The enzymatic activity of TPI is affected by nitrotyrosination

Substrate	GAP		DHAP	
	Control TPI	Nitro-TPI	Control TPI	Nitro-TPI
K_m (mM)	1.65 ± 0.41	0.62 ± 0.16	0.84 ± 0.42	1.11 ± 0.15
$V_{max} \times 10^{-3}$ (mM·s^{-1})	2.16 ± 1.32	0.2 ± 0.04	0.14 ± 0.04	0.09 ± 0.01
$K_{cat} \times 10^{5}$ (min^{-1})	5.75 ± 3.51	0.53 ± 0.21	0.11 ± 0.28	0.07 ± 0.01
$K_{cat}/K_m \times 10^{5}$ (mM^{-1} min^{-1})	3.49 ± 2.30	0.87 ± 0.41	0.13 ± 0.07	0.06 ± 0.02
MG formation (percent respect to control)	100	211.18 ± 21.16	100	132.68 ± 5.66

For the enzymatic assays 3 ng of GAP and 10 ng of DHAP were used. MG measurement was made with 0.5 mM GAP or 2.4 mM DHAP after 10 min of adding substrate. The number of experiments was 3–6.

TPI nitrotyrosination induces its aggregation

TPI belongs to the class of the α/β barrel enzymes (Dabrowska *et al*., 1978; Pompliano *et al*., 1990). TPI contains β strands (Dabrowska *et al*., 1978) and a TPI fragment 186–218 from the N-terminal of region III is able to form amyloid-like fibrils *in vitro* (Contreras *et al*., 1999). Turbidometric analysis of TPI in solution demonstrated rapid induction of TPI aggregation upon nitrotyrosination with SIN-1 (Fig. 4A), resulting in the appearance of multimeric TPI bands of higher electrophoretic mobility (Fig. 4B). RNAse (also a dimeric protein with several Tyr) did not aggregate upon SIN-1 treatment, suggesting that this effect was rather specific for TPI (Supplementary Fig. S4). TEM analysis identified large aggregates of nitro-TPI (Fig. 4D), which were not appearing in the control TPI reaction (Fig. 4C). TPI also aggregates *in vivo*. When TPI was immunoprecipitated from human cortex (Fig. 4E and F; Supplementary Fig. S5) and hippocampus (Supplementary Fig. S5), large protein aggregates were obtained from Alzheimer's disease brains and not from healthy controls. Nitro-TPI aggregates generated *in vitro* exhibited positive thioflavin staining at day five (insets Fig. 4C and D), further confirming that TPI aggregates displayed β-sheet structure (Grabowski *et al*., 2001). These nitro-TPI aggregates continue to produce toxic methylglyoxal. We reasoned that these TPI aggregates, due to their amyloid-like structure, might also act as nucleation centres for fibrillation of other intracellular proteins in the cell (inset Fig. 4F). TPI aggregation could also affect substrate access to and occupancy of the catalytic centre, thereby, contributing to the increased methylglyoxal production.

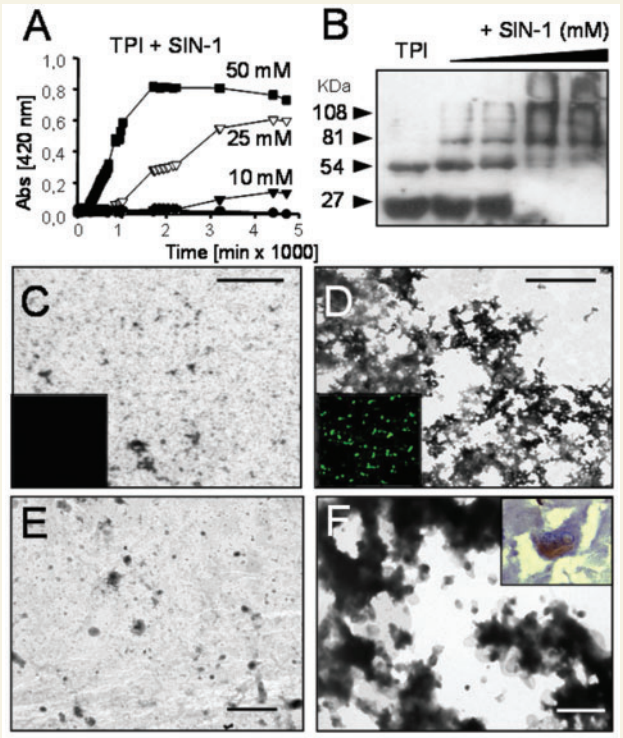

Figure 4 The nitrotyrosination of TPI is inducing its aggregation. (**A**) The *in vitro* aggregation was followed by a turbidometric assay of TPI (filled circle) and TPI+SIN-1 [10 mM (filled inverted triangle), 25 mM (open inverted triangle), 50 mM (filled square)] followed by measuring A_{402}. (**B**) Western blot detection with an anti-TPI antibody of TPI nitrotyrosinated with SIN-1 (48 h) demonstrated the presence of TPI oligomers proportional to increasing concentrations of SIN-1 (0, 10, 25 and 50 mM). TEM images of immunoprecipitates were obtained using anti-TPI antibody in samples from (**C**) control TPI and (**D**) TPI nitrotyrosinated *in vitro*; and, human cortex from (**E**) healthy and (**F**) Alzheimer's disease patients. Immunoprecipitates of (inset **C**) normal TPI were negative for thioflavine T staining but they were positive for (inset **D**) nitro-TPI indicating the folding in β-sheet structure (inset **F**). The intracellular aggregation of TPI was demonstrated in cells from sections of Alzheimer's disease patient cortex. Bars are 1 μm (**C** and **D**) and 2 μm (**E** and **F**).

Nitrotyrosinated TPI interacts with tau protein to form paired helical filaments

Mutations in TPI make it more prone to associate with and influence assembly of brain microtubules (Orosz *et al*., 2000). Therefore, we addressed the possibility that nitrotyrosinated TPI might provide a nucleation centre for tau aggregation and subsequent paired helical filament formation. Human neuroblastoma cells were treated with increasing concentrations of Aβ and proteins were immunoprecipitated with anti-TPI antibody. Tau-positive material was present in the immunoprecipitates indicating that tau becomes associated to nitroTPI in an Aβ dose-dependent pattern (Fig. 5A). This interaction was critically dependent on the nitrotyrosination of TPI, as treatment with 2-phenyl-4,4,5,5,-tetramethylimidazoline-1-oxyl 3-oxide (PTIO; a NO scavenger) or the free radical scavenger (trolox) markedly reduced the binding of tau to TPI in the presence of Aβ (Fig. 5B). The unspecific TPI binding to protein G sepharose was excluded (Fig. 5C, E, F and G). In tissue slides from Alzheimer's disease cortex, we have found that TPI co-localizes with tau (Fig. 6A). In triple transgenic mice that overexpressed APP, PS1 and tau (Oddo *et al*., 2003), we found a massive presence of tau (50 kDa isoform) in the TPI immunoprecipitated material (Figs 5E, 6B and Supplementary Fig. S6). Similarly, tau immunoreactivity associated with immunoprecipitated TPI was detected in samples obtained from human Alzheimer's disease cortex but not from healthy subjects (Figs 5F, 6B and Supplementary Fig. S6). Tau binding to TPI seems rather specific for Alzheimer's disease brain as cortex samples from Parkinson's disease and frontotemporal dementia patients turned out to be negative for tau in the TPI immunoprecipitates (Fig. 5G). TPI immunoprecipitates tau in both Alzheimer's disease brains and transgenic mice but no another protein highly expressed in brain such as syntaxin 1A (Fig. 6C).

We further investigated how nitro-TPI affected tau aggregation *in vitro*. TPI and nitro-TPI were incubated with tau protein and samples were analysed by Atomic Force Microscopy (Fig. 7A–D) and TEM (Fig. 7F and G). Abundant paired helical filament-like structures were found in samples containing nitro-TPI plus tau

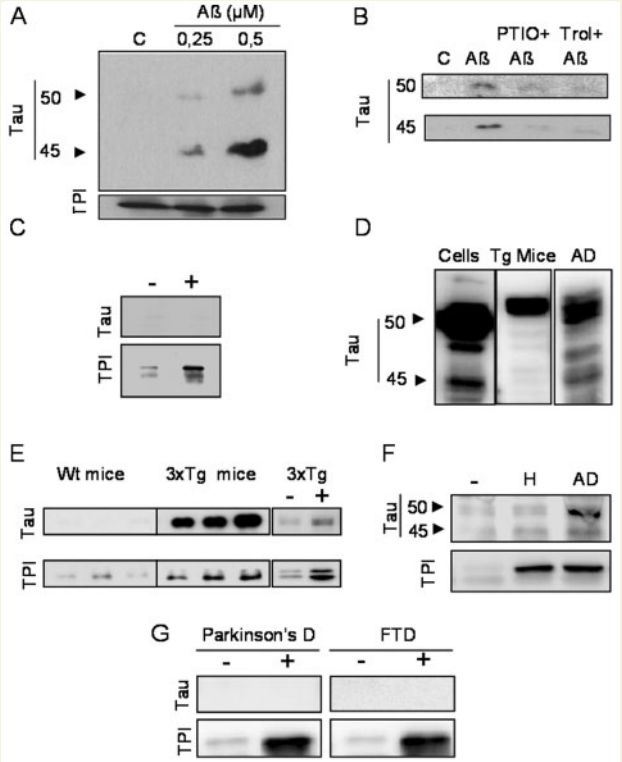

Figure 5 Tau protein coimmunoprecipitates with nitro-TPI. All the cell lysates and tissue samples were immunoprecipitated with an anti-TPI antibody. (**A**) SH-SY5Y cells were treated with two sub-lethal concentrations of Aβ fibrils. Western blots were performed with antibodies anti-tau and anti-TPI. (**B**) SH-SY5Y cells were pretreated with PTIO (a NO scavenger) or Trolox (a free radical scavenger) before adding the Aβ fibrils. A Western blot was performed with an anti-tau antibody. (**C**) Controls were performed to assay the unspecific TPI binding to protein G sepharose (lane −) compared with the normal anti-TPI immunoprecipitation (lane +). (**D**) Total lysates from SH-SY5Y cells, 3xTg mice and Alzheimer's disease cortex were applied to Western blot to identify the most abundant tau isoforms. (**E**) Co-immunoprecipitation of tau (50 kDa) with TPI was also assessed in three different mice overexpressing APP, PS1 and human tau. The respective controls for the immunoprecipitation without anti-TPI (lane −) and with anti-TPI (lane +) are also shown in the panel. (**F**) The presence of tau in the TPI immunoprecipitates obtained from healthy and Alzheimer's disease cortex was analysed by immunoblotting with antibodies anti-tau and anti-TPI. The control for the non-specific binding to protein *G*-sepharose is shown in the panel (lane −). (**G**) TPI immunoprecipitates obtained from frontal cortex of Parkinson's disease and frontotemporal dementia patients are shown with the respective controls for the non-specific binding to protein *G*-sepharose.

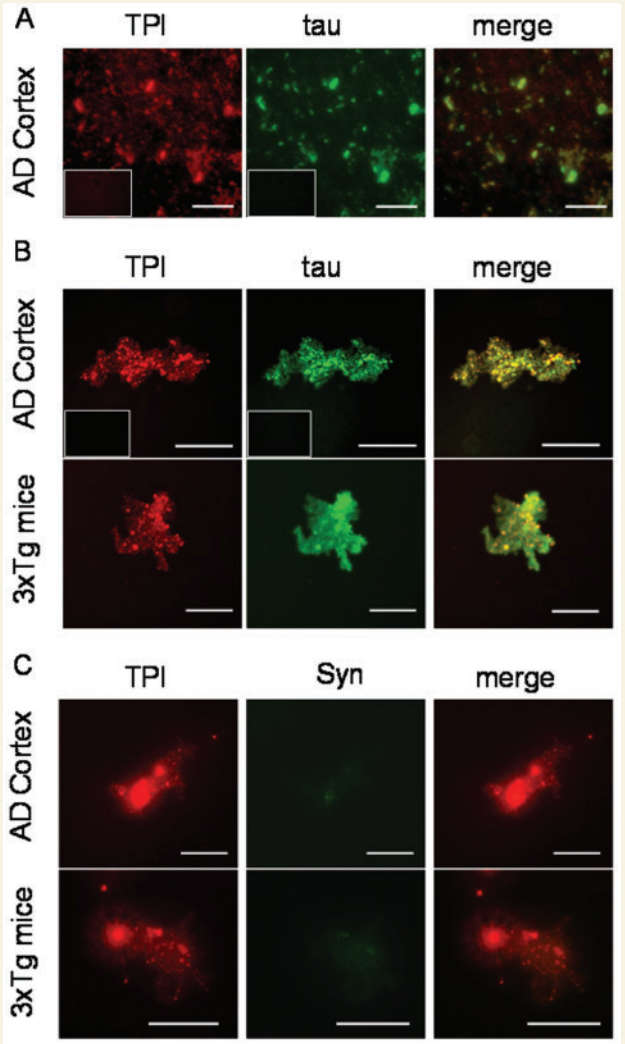

Figure 6 Co-localization of TPI and tau protein in brain samples. (**A**) TPI and tau were co-immunolabelled in tissue slides from Alzheimer's disease cortex. (Inset **A**) Controls with secondary antibody were performed for both TPI and tau. (**B**) TPI immunoprecipitates obtained from Alzheimer's disease cortex and triple transgenic mice overexpressing APP, PS1 and tau were immunolabelled with anti-TPI and tau. (Inset **B**) Controls with secondary antibody were performed for both TPI and tau. (**C**) TPI immunoprecipitates obtained from Alzheimer's disease cortex and triple transgenic mice were immunolabelled with anti-TPI and anti-syntaxin 1A as a control of the specificity of the tau binding to TPI. Bars are 100 µm (Alzheimer's disease cortex; **A** and **B**), 50 µm (3xTg mice; **B**) and 37.5 µm (**C**).

(Fig. 7C and D) with the characteristic twisted fibrils structure that is also seen in twisted paired helical filaments in Alzheimer's disease brains (Fig. 7D) (Herzig *et al*., 2006). Samples containing tau plus unmodified TPI showed only few fibrillar aggregates, not displaying paired helical filament structure (Fig. 7A and B). In control experiments using another nitrotyrosinated cytoplasmic protein, nitro-human RNAse 3, no paired helical filament formation was observed, indicating specificity of our observations (Supplementary Fig. S7). In agreement with the atomic force microscopy data, Western blot analysis of the samples revealed that, unlike control TPI, nitro-TPI induced stable paired helical filaments that did not enter into the SDS gel (Fig. 7E). Nitro-TPI promoted paired helical filaments at very low tau concentrations (65 nM) which are well below the concentrations (1–10 µM) used in previous studies to trigger paired helical filament formation with

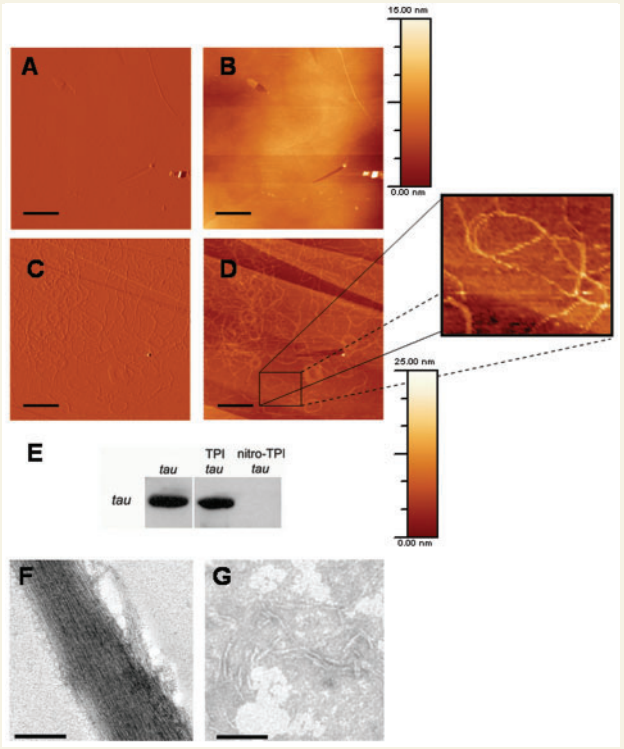

Figure 7 Fibrillation of tau into paired helical filaments demonstrated by atomic force microscopy and TEM. Tau was incubated for 4 days in the presence of (**A** and **B**) TPI or (**C** and **D**) nitro-TPI at a 1 : 1 (w/w) ratio and seeded on graphite surfaces for atomic force microscopy visualization. (**A** and **B**) Tau-control TPI samples show few fibrils without defined structure. (**C** and **D**) Tau-nitro-TPI samples exhibit abundant fibrils that are similar in morphology to paired helical filaments when their topography is visualized. (**E**) Western blot detection of tau in the samples used for atomic force microscopy studies: control of tau alone, TPI+tau and nitro-TPI+tau. (**F** and **G**) TEM images of the fibrils found in tau-nitro-TPI samples.

exogenous triggers such as heparin, anionic surfactants and calcium (Grabowski *et al*., 2001).

Discussion

In the present work, we have studied the possible pathophysiological relevance of TPI nitrotyrosination in Alzheimer's disease. First, we have demonstrated that Aβ induces TPI nitrotyrosination in neuronal cells. Accordingly, TPI nitrotyrosination was also observed in the brain of Alzheimer's disease patients and mice overexpressing both amyloid precursor protein (APP) and presenilin 1 (PS1), but not in control brains. Second, the Aβ-induced nitrotyrosination of TPI affects its function and could result in inefficient glycolysis in Alzheimer's disease. In fact, ATP depletion has been reported in Alzheimer's disease patients (Hoyer *et al*., 1988). TPI nitrotyrosination decreased both isomerase activities, which slows the glycolytic flow and ATP formation and could result in decreased production of acetyl-coenzyme A (acetyl-CoA). A reduction in the bioavailability of acetyl-CoA, a precursor of acetylcholine synthesis, could contribute to the characteristic cholinergic deficit in Alzheimer's disease. Moreover, TPI is the only glycolytic enzyme that has been implicated in neurodegeneration (Eber *et al*., 1991; Valentin *et al*., 2000; Ovadi *et al*., 2004). In all these studies high levels of DHAP were found as a result of decreased TPI isomerase activity. DHAP is the main source for toxic methylglyoxal production. Methylglyoxal is a very unstable intermediate and toxic triose involved in AGEs formation and implicated before in Alzheimer's disease pathogenesis (Ahmed *et al*., 2003). TPI prevents methylglyoxal production by folding its loop 6 over the catalytic centre when the substrate binds. Nitration of Y164 keeps loop 6 open via a hydrogen bond with T168, allowing the entry of water into the active site resulting in the hydrolysis of the phosphate of the enediol intermediate to yield methylglyoxal.

On the other hand, mutated TPI becomes misfolded forming several β strands (Rice *et al*., 1990) and such misfolded protein could also promote neurodegenerative disease (Olah *et al*., 2002). Some mutations in TPI make it more prone to associate with brain microtubules, which influence their polymerization (Orosz *et al*., 2000). Interestingly, a fragment of TPI is structurally homologous to the Aβ peptide and is able to form amyloid *in vitro* (Contreras *et al*., 1999). We have demonstrated that nitrotyrosination induces the aggregation of TPI. This nitrotyrosinated TPI forms large structures with β-sheet folds that are induced in neurons cultured *in vitro*, in the presence of Aβ, and, importantly, are observed in cortex from Alzheimer's disease brain. The large size of nitrotyrosinated TPI aggregates make them resistant to degradation by the proteosome. They can then grow and act as intracellular 'seeds' for the fibrillation of other proteins due to the amyloid-like structure.

Neurofibrillary tangle, formation due to tau aggregation, is considered a key event in Alzheimer's disease neurodegeneration. Neurons bearing neurofibrillary tangles are not necessarily dead but unable to communicate with other neurons due to the disruption of the cytoskeleton. Neurofibrillary tangles are downstream of Aβ action since mutations in human amyloid precursor protein produce an early onset of Alzheimer's disease with neurofibrillary tangles present in the brains of these patients (Cras *et al*., 1998; Sturchler-Pierrat and Sommer, 1999). On the other hand, mutations in human tau producing frontal dementia do not show any alteration of Aβ (Yancopoulou *et al*., 2003). Despite all this evidence relating Aβ to neurofibrillary tangle formation, there is no experimental explanation for the link between these two major events in Alzheimer's disease. The participation of cyclin-dependent kinases (Maccioni *et al*., 2001) or glycogen synthase kinase-3β signalling (Bhat *et al*., 2004) are among the few hypotheses attempting to explain this link at a molecular level, although it remains unexplained how Aβ can trigger the generation of paired helical filaments. Hyperphosphorylation of tau has been proposed to mediate paired helical filament formation, but a phosphorylation-independent mechanism is also involved in the formation of paired helical filaments (Goedert *et al*., 1996). We demonstrate here a direct association between paired helical filaments and nitrotyrosinated TPI in Alzheimer's disease brains. This association appears rather

specific as a limited survey of material obtained from Parkinson's disease and frontotemporal dementia did not reveal association of TPI and tau in co-immunoprecipitation experiments. Therefore, and based on our cellular experiments, we speculate that the nitrative stress induced by Aβ in Alzheimer's disease is critical for nitro-TPI induced tau aggregation. Moreover, nitrotyrosinated TPI aggregates induce the fibrillation of tau to form paired helical filaments in the absence of tau phosphorylation. It is conceivable that hyperphosphorylation of tau is an event posterior to paired helical filament formation. The conformational changes of tau aggregated into paired helical filaments could indeed expose the phosphorylation sites to kinases.

In summary, our data show that nitrotyrosinated TPI might affect multiple mechanisms relevant to the pathophysiology of Alzheimer's disease. It compromises cellular metabolism by reducing the glycolytic flow and ATP generation and by increasing the production of methylglioxal. More interestingly, nitro-TPI adopts a β-sheet structure with the capability of triggering paired helical filament formation in the absence of tau phosphorylation. Finally, our results also provide a mechanistic explanation linking oxidative stress, which is at the core of the etiopathogenic loop described in sporadic Alzheimer's disease (Frederikse *et al*., 1996; Miranda *et al*., 2000; Opazo *et al*., 2002), via the production of peroxynitrite and nitrotyrosination of TPI, to Aβ-induced toxicity and tau pathology.

Supplementary material

Supplementary material is available at *Brain* online.

Acknowledgements

We acknowledge to the Banc de Teixit Neurologic del Hospital Clinic de Barcelona and to Unidad de Neuropatología y Banco de Cerebros of Fundación Hospital Alcorcón for providing the brain samples. We acknowledge David Andreu for technical support and Dr Frank LaFerla for providing us mice material. Finally, we acknowledge the computer resources, technical expertise and assistance provided by the Barcelona Supercomputing Center.

Funding

Spanish Ministerio de Sanidad (FIS: PRO1208; Red HERACLES RD06/0009/002); Educación y Ciencia (BIO2005-01591, SAF2006-4973, CSD2006-00012); Generalitat de Catalunya (GSR2005-266; 2005-SGR00037); EC funded STREP project QosCosGrid (IST-033883); VPH NOE (ICT-223920); Methusalem grant of the Flemish government (to lab of BDS); VIB and KUL (to lab of BDS).

References

Ahmed N, Battah S, Karachalias N, Babaei-Jadidi R, Horanyi M, Baroti K, et al. Increased formation of methylglyoxal and protein glycation, oxidation and nitrosation in triosephosphate isomerase deficiency. Biochim Biophys Acta 2003; 1639: 121–32.

Alonso AC, Li B, Grundke-Iqbal I, Iqbal K. Mechanism of tau-induced neurodegeneration in Alzheimer disease and related tauopathies. Curr Alzheimer Res 2008; 5: 375–84.

Bhat RV, Budd Haeberlein SL, Avila J. Glycogen synthase kinase 3: a drug target for CNS therapies. J Neurochem 2004; 89: 1313–7.

Brion JP, Couck AM, Passareiro E, Flament-Durand J. Neurofibrillary tangles of Alzheimer's disease: an immunohistochemical study. J Submicrosc Cytol 1985; 17: 89–96.

Chang E, Kim S, Yin H, Nagaraja HN, Kuret J. Pathogenic missense MAPT mutations differentially modulate tau aggregation propensity at nucleation and extension steps. J Neurochem 2008; 107: 1113–23.

Chirita CN, Necula M, Kuret J. Anionic micelles and vesicles induce tau fibrillization in vitro. J Biol Chem 2003; 278: 25644–50.

Coma M, Guix FX, Uribesalgo I, Espuna G, Sole M, Andreu D, et al. Lack of oestrogen protection in amyloid-mediated endothelial damage due to protein nitrotyrosination. Brain 2005; 128: 1613–21.

Contreras CF, Canales MA, Alvarez A, De Ferrari GV, Inestrosa NC. Molecular modeling of the amyloid-beta-peptide using the homology to a fragment of triosephosphate isomerase that forms amyloid in vitro. Protein Eng 1999; 12: 959–66.

Cras P, van Harskamp F, Hendriks L, Ceuterick C, van Duijn CM, Stefanko SZ, et al. Presenile Alzheimer dementia characterized by amyloid angiopathy and large amyloid core type senile plaques in the APP 692Ala–>Gly mutation. Acta Neuropathol (Berl) 1998; 96: 253–60.

Dabrowska A, Kamrowska I, Baranowski T. Purification, crystallization and properties of triosephosphate isomerase from human skeletal muscle. Acta Biochim Pol 1978; 25: 247–56.

Del Toro D, Coma M, Uribesalgo I, Guix FX, Muñoz FJ. The amyloid beta-protein precursor and Alzheimer's disease-therapeutic approaches. Curr Med Chem 2005; 5: 271–83.

Eber SW, Pekrun A, Bardosi A, Gahr M, Krietsch WK, Kruger J, et al. Triosephosphate isomerase deficiency: haemolytic anaemia, myopathy with altered mitochondria and mental retardation due to a new variant with accelerated enzyme catabolism and diminished specific activity. Eur J Pediatr 1991; 150: 761–6.

Frederikse PH, Garland D, Zigler JS, Piatigorsky J. Oxidative stress increases production of beta-amyloid precursor protein and beta-amyloid (Abeta) in mammalian lenses, and Abeta has toxic effects on lens epithelial cells. J Biol Chem 1996; 271: 10169–74.

Goedert M, Jakes R, Spillantini MG, Hasegawa M, Smith MJ, Crowther RA. Assembly of microtubule-associated protein tau into Alzheimer-like filaments induced by sulphated glycosaminoglycans. Nature 1996; 383: 550–3.

Gotz J, Chen F, van Dorpe J, Nitsch RM. Formation of neurofibrillary tangles in P301l tau transgenic mice induced by Abeta 42 fibrils. Science 2001; 293: 1491–5.

Grabowski TJ, Cho HS, Vonsattel JP, Rebeck GW, Greenberg SM. Novel amyloid precursor protein mutation in an Iowa family with dementia and severe cerebral amyloid angiopathy. Ann Neurol 2001; 49: 697–705.

Guix FX, Uribesalgo I, Coma M, Muñoz FJ. The physiology and pathophysiology of nitric oxide in the brain. Prog Neurobiol 2005; 76: 126–52.

Herzig MC, Van Nostrand WE, Jucker M. Mechanism of cerebral beta-amyloid angiopathy: murine and cellular models. Brain Pathol 2006; 16: 40–54.

Hoyer S, Oesterreich K, Wagner O. Glucose metabolism as the site of the primary abnormality in early-onset dementia of Alzheimer type? J Neurol 1988; 235: 143–8.

Iqbal K, Zaidi T, Thompson CH, Merz PA, Wisniewski HM. Alzheimer paired helical filaments: bulk isolation, solubility, and protein composition. Acta Neuropathol 1984; 62: 167–77.

Keil U, Bonert A, Marques CA, Scherping I, Weyermann J, Strosznajder JB, et al. Amyloid beta-induced changes in nitric oxide production and

mitochondrial activity lead to apoptosis. J Biol Chem 2004; 279: 50310–20.

Kuhla B, Luth HJ, Haferburg D, Boeck K, Arendt T, Munch G. Methylglyoxal, glyoxal, and their detoxification in Alzheimer's disease. Ann NY Acad Sci 2005; 1043: 211–16.

Kuret J, Congdon EE, Li G, Yin H, Yu X, Zhong Q. Evaluating triggers and enhancers of tau fibrillization. Microsc Res Tech 2005; 67: 141–55.

Liou YC, Sun A, Ryo A, Zhou XZ, Yu ZX, Huang HK, et al. Role of the prolyl isomerase Pin1 in protecting against age-dependent neurodegeneration. Nature 2003; 424: 556–61.

Maccioni RB, Muñoz JP, Barbeito L. The molecular bases of Alzheimer's disease and other neurodegenerative disorders. Arch Med Res 2001; 32: 367–81.

Masters CL, Beyreuther K. Alzheimer's centennial legacy: prospects for rational therapeutic intervention targeting the Abeta amyloid pathway. Brain 2006; 129: 2823–39.

Miranda S, Opazo C, Larrondo LF, Muñoz FJ, Ruiz F, Leighton F, et al. The role of oxidative stress in the toxicity induced by amyloid beta-peptide in Alzheimer's disease. Prog Neurobiol 2000; 62: 633–48.

Mudher A, Lovestone S. Alzheimer's disease-do tauists and baptists finally shake hands? Trends Neurosci 2002; 25: 22–6.

Oddo S, Caccamo A, Shepherd JD, Murphy MP, Golde TE, Kayed R, et al. Triple-transgenic model of Alzheimer's disease with plaques and tangles: intracellular Abeta and synaptic dysfunction. Neuron 2003; 39: 409–21.

Olah J, Orosz F, Keseru GM, Kovari Z, Kovacs J, Hollan S, et al. Triosephosphate isomerase deficiency: a neurodegenerative misfolding disease. Biochem Soc Trans 2002; 30: 30–8.

Opazo C, Huang X, Cherny RA, Moir RD, Roher AE, White AR, et al. Metalloenzyme-like activity of Alzheimer's disease beta-amyloid. Cu-dependent catalytic conversion of dopamine, cholesterol, and biological reducing agents to neurotoxic H_2O_2. J Biol Chem 2002; 277: 40302–8.

Orosz F, Wagner G, Liliom K, Kovacs J, Baroti K, Horanyi M, et al. Enhanced association of mutant triosephosphate isomerase to red cell membranes and to brain microtubules. Proc Natl Acad Sci USA 2000; 97: 1026–31.

Otth C, Concha II, Arendt T, Stieler J, Schliebs R, Gonzalez-Billault C, et al. AbetaPP induces cdk5-dependent tau hyperphosphorylation in transgenic mice Tg2576. J Alzheimers Dis 2002; 4: 417–30.

Ovadi J, Orosz F, Hollan S. Functional aspects of cellular microcompartmentation in the development of neurodegeneration: mutation induced aberrant protein-protein associations. Mol Cell Biochem 2004; 256–257: 83–93.

Pompliano DL, Peyman A, Knowles JR. Stabilization of a reaction intermediate as a catalytic device: definition of the functional role of the flexible loop in triosephosphate isomerase. Biochemistry 1990; 29: 3186–94.

Rice PA, Goldman A, Steitz TA. A helix-turn-strand structural motif common in alpha-beta proteins. Proteins 1990; 8: 334–40.

Richard JP. Mechanism for the formation of methylglyoxal from triosephosphates. Biochem Soc Trans 1993; 21: 549–53.

Sturchler-Pierrat C, Sommer B. Transgenic animals in Alzheimer's disease research. Rev Neurosci 1999; 10: 15–24.

Valentin C, Cohen-Solal M, Maquat L, Horanyi M, Inselt-Kovacs M, Hollan S. Identical germ-line mutations in the triosephosphate isomerase alleles of two brothers are associated with distinct clinical phenotypes. C R Acad Sci III 2000; 323: 245–50.

Wszolek ZK, Tsuboi Y, Ghetti B, Pickering-Brown S, Baba Y, Cheshire WP. Frontotemporal dementia and parkinsonism linked to chromosome 17 (FTDP-17). Orphanet J Rare Dis 2006; 9: 1–30.

Yancopoulou D, Crowther RA, Chakrabarti L, Gydesen S, Brown JM, Spillantini MG. Tau protein in frontotemporal dementia linked to chromosome 3 (FTD-3). J Neuropathol Exp Neurol 2003; 62: 878–82.